Journal of Porous Materials (2024) 31:1789–1800
https://doi.org/10.1007/s10934-024-01633-5

A novel high-efficiency In-based catalyst for ethylbenzene dehydrogenation with CO_2

Quanhua Wang[1,2] · Ruiqi Wei[2] · Meng Pan[3] · Yanchao Liu[2] · Lichen Zhang[2] · Jiajun Zheng[2] · Shuwei Chen[2] · Yuhao Zong[1] · Hu Wang[1] · Kaifei Yin[1] · Yanwei Yue[1] · Jinke Li[1]

Published online: 21 May 2024

Abstract
A series of binary In_2O_3/S (S = Al_2O_3, SiO_2, and MgO) catalysts were fabricated by an incipient-wetness impregnation method, which were firstly applied in the ethylbenzene dehydrogenation under the presence of CO_2 (EBDH-CO_2). The synthesized catalysts were systematically characterized by X-ray diffraction (XRD), scanning electron microscopy (SEM), transmission electron microscopy (TEM), N_2 adsorption–desorption isotherm, temperature-programmed desorption of NH_3 and CO_2 (NH_3/CO_2-TPD), temperature-programmed reduction of H_2 (H_2-TPR), and X-ray photoelectron spectroscopy (XPS). It is found that the support can strongly impact on the crystalline phase, the dispersity, and the reduction properties of In_2O_3. The catalytic tests during the EBDH-CO_2 show that as compared to In_2O_3/MgO and In_2O_3/SiO_2 with the merely existence of bulk In_2O_3 particles, the In_2O_3/Al_2O_3 catalyst gives the highest catalytic activity and good stability, which can be principally ascribed to the synergistic effect of the bulk In_2O_3 and in situ metallic In formed by the reduction of the well-dispersed In_2O_3 on the Al_2O_3 surface. It therefore affirms that attaining an appropriate support to disperse the active phase In_2O_3 becomes the decisive factor to achieve both superior catalytic activity and satisfied selectivity towards styrene.

Keywords Ethylbenzene dehydrogenation · Carbon dioxide · In-containing catalysts · Al_2O_3 support · Synergistic effect

1 Introduction

The constant depletion of fossil reserves and the stringent environmental regulations have impelled tremendous endeavors toward highly efficient catalysts to obtain high value-added olefins from hydrocarbons in a green manner [1, 2]. Styrene (ST), as a versatile chemical feedstock extensively used for the manufacture of polymer materials, is commercially obtained by the direct dehydrogenation of ethylbenzene (EB) using Fe-K-based catalysts [3–5]. In such a catalytic system, high EB conversion and ST selectivity can be only achieved in the high temperature range of 600–650 °C. Meanwhile, a vast amount of superheated steam (steam: EB = 6–13:1 in molar) must be supplied concurrently as a co-feed to decelerate the catalyst deactivation [6, 7]. As a consequence, the high energy consumption and the requirement for abundant water input have become the primary obstacles to industrial application. More recently, taking environmental and economic interests into account, ethylbenzene dehydrogenation with CO_2 as a mild oxidant (EBDH-CO_2) has captured much attention because of its advantages of the lower energy consumption, overcoming the thermodynamic limitation, and prolonging the catalytic lifespan [4]. The highlight of this reaction is that CO_2 can react with hydrogen produced by the direct dehydrogenation of EB via a reverse water–gas shift (RWGS) reaction ($CO_2 + H_2 \leftrightarrow CO + H_2O$), which can in turn promote the EBDH-CO_2 process. Unfortunately, the aforementioned commercial Fe-K oxide catalysts do not work efficaciously in this new reaction system [8, 9]. To overcome this drawback, researchers have devoted impressive efforts to exploiting the high-efficiency catalysts for accessing EBDH-CO_2.

✉ Quanhua Wang
wangquanhuatyut@163.com

✉ Shuwei Chen
csw603@163.com

[1] Datang Nanjing Environmental Protection Technology Co., Ltd., Nanjing 211111, Jiangsu, China

[2] Research Centre of Energy Chemical & Catalytic Technology, Taiyuan University of Technology, Taiyuan 030024, People's Republic of China

[3] College of Biological and Chemical Engineering, Anhui Polytechnic University, Wuhu 241000, China

Although numerous catalysts, including V-, Cr-, Ce-, and Mn-based oxides [10–14], are found to be highly active towards EBDH-CO_2, the rapid deactivation even within a few hours of time-on-stream is difficult to circumvent due to coke formation. Thus, the development of new metal or metal-oxide catalytic materials, achieving the efficient improvement of the catalytic activity and stability of EBDH-CO_2.

Indium oxide (In_2O_3) as an important member of Group IIIA metal oxides has been frequently applied in optical guides, photocatalysts, and electrical condensers [15–19] because it has some charming properties, including intrinsic oxygen vacancies facilitating the electronic conductivity. In recent years, indium materials have been widely utilized as novel efficient catalysts for some alkanes (such as ethane and propane) dehydrogenation and ethanol dehydration reactions [20–27]. Wang et al. [20] reported a highly stable In-HY catalyst for ethane dehydrogenation reaction, obtaining nearly 100% selectivity to ethene and reaching up to 60% ethene yield, arising from the formed In single atoms by replacing the protons of supercages in HY zeolite which were found to be active centers for achieving the ethane activation. Chen et al. [21] demonstrated that the prominent catalytic activity of propane dehydrogenation using CO_2 as an oxidant was obtained over In_2O_3/Al_2O_3 catalyst, further revealing that in situ metallic In, which was formed by the reduction of the highly dispersed In_2O_3 under the reductive atmosphere, was well responsible for the propane dehydrogenation. Zonetti et al. [22] found that In_2O_3/ZrO_2 catalyst could be considered as a promising catalyst for the preparation of isobutene from ethanol owing to the interdiffusion process between In_2O_3 and ZrO_2, which was conducive to generating more anionic vacancies, leading to an increase in the redox properties of In_2O_3 which allowed for a high activity for the intermediate acetone generation. However, to the best of the author's knowledge, the catalytic behavior of EBDH-CO_2 over In-based catalysts has not been reported to date.

It has been widely acknowledged that except for the specific active components, the nature of support plays a pivotal role in modulating the physicochemical properties (dispersion, distribution, and surface structure, etc.) of active species, being able to further govern the catalytic performance of a given catalyst [26, 28, 29]. In which, the acid–base characteristics of the catalyst, which are predominantly derived from support, are the vital factors affecting the adsorption and activation of EB and CO_2 when involved with EBDH-CO_2 [30]. In this work, to gain insight into the role of the support on the physicochemical properties of the In_2O_3-based materials, three representative oxide supports (Al_2O_3, MgO, and SiO_2) with the well-differentiated acid–base and structural properties are therefore employed. The structure and redox properties of the as-synthesized catalysts were characterized by performing a series of analytical techniques including X-ray diffraction (XRD), scanning electron microscopy (SEM), transmission electron microscopy (TEM), N_2 adsorption–desorption isotherm, temperature-programmed desorption of NH_3 and CO_2 (NH_3/CO_2-TPD), temperature-programmed reduction of H_2 (H_2-TPR), and X-ray photoelectron spectroscopy (XPS). Furthermore, the catalytic performances of EBDH-CO_2 are investigated in detail and a possible reaction pathway is proposed.

2 Experimental

2.1 Catalyst preparation

A series of binary oxides were synthesized by incipient wetness impregnation method using a solution of $In(NO_3)\cdot 4H_2O$ (Macklin, 99.99%). MgO was purchased from Tianjin Kermel Chemical Reagent Co., Ltd. Al_2O_3 and SiO_2 were obtained from the Institute of Coal Chemistry, Chinese Academy of Science. Before impregnation, these supports were calcined at 550 ℃ for 6 h to remove the adsorbed gas molecules and then impregnated with the loading of 10 wt% In_2O_3. In fact, the In_2O_3 loading of all samples is about 9.5 wt% based on the ICP results (Table 1) which is close to the theoretical value (10 wt.%). The as-prepared samples were placed at room temperature for 24 h, followed by drying at 120 ℃ for 12 h and calcining in air at 550 ℃ for 6 h. The final obtained catalyst was labeled as In_2O_3/S, where "S" represents the selected support. For comparison, pure phase In_2O_3 was also fabricated by direct calcination of indium precursor ($In(NO_3)\cdot 4H_2O$) at 550 ℃ for 6 h.

2.2 Catalyst characterization

X-ray powder diffraction (XRD) patterns were performed on a Shimadzu X-ray diffractometer. The average crystallite sizes of the samples were calculated by using the Scherrer Formula: $D = K\lambda/\beta\cos\theta$, where D is the average sizes of the crystallite domains, K is a dimensionless shape factor, λ is the wavelength, β is the line broadening at half the maximum intensity, and θ is the Bragg diffraction angle.

The morphology and crystal of the samples were conducted on Hitachi S4800 scanning electron microscopy (SEM) and JEM-2100F transmission electron microscope (TEM). The In_2O_3 loading amount of the as-prepared samples was determined from inductively coupled plasma performed by a Thermo IRIS Intrepid II XSP atomic emission spectrometer (ICP-AES). The structural parameters of the as-synthesized products were obtained using a NOVA 1200e sorption analyzer. Pore size distributions were obtained with the DFT method on the adsorption branch using cylindrical pore NLDFT (Non-Local Density Functional Theory) model. H_2 chemisorption was

Table 1 Physicochemical properties of samples

Sample	In_2O_3 loading[a] (wt.%)	S_{BET}[b] (m^2/g)	V_{pore}[c] (cm^3/g)	D_{pore}[d] (nm)	Average crystallite size of In_2O_3[e] (nm)
In_2O_3	–	13	0.06	16.9	–
Al_2O_3	–	247	0.63	10.1	–
In_2O_3/Al_2O_3	9.45	195	0.49	9.5	–
SiO_2	–	156	0.91	23.3	–
In_2O_3/SiO_2	9.53	134	0.81	24.1	18.4
MgO	–	49	0.32	26.2	–
In_2O_3/MgO	9.48	45	0.29	25.2	9.4

[a]Determined by inductively coupled plasma (ICP)

[b]Calculated by the BET method

[c]The total pore volume is calculated from N_2 adsorption capacity at a relative pressure of 0.99

[d]The average pore size is determined by the BJH method

[e]Calculated by the Scherrer equation

undertaken on a Micromeritics AutoChem II 2920. 0.1 g of the sample was reduced with 10% H_2/Ar at 450 ℃ for 2 h and purged in pure Ar for 1 h. Thereafter, the temperature was decreased to 30 ℃. H_2 pulses were performed by a calibrated on-line sampling value. The acidity and basicity of the samples were respectively studied by temperature-programmed desorption (TPD) of NH_3 and CO_2, using a TP-5076 measurement equipped with a thermal conductivity detector (TCD). X-ray photoelectron spectroscopy (XPS) was collected on an EscaLab 250 spectrometer using an Al-Kα (1486.7 eV) as the excitation source. The reducibility of the samples was determined by hydrogen temperature-programmed reduction (H_2-TPR) on a Micromeritics Autochem 2920 instrument.

2.3 Catalytic testing

The catalytic performance of EBDH-CO_2 was carried out in a fixed-bed microreactor at atmospheric pressure. 0.3 g of the calcined catalyst sieved to 40–60 mesh was loaded into a stainless-steel tube with an inner diameter of 6 mm. Before each test, the catalyst was activated at 550 ℃ for 2 h with a ramping rate of 5 ℃/min in flowing of N_2 (20 mL/min). Subsequently, the N_2 flow was switched to CO_2 (20 mL/min). The catalyst was then maintained at reaction temperature of 550 ℃ for 15 min in a CO_2 flow. After that, ethylbenzene as a reactant was instilled by a peristaltic pump, maintaining a weight hourly space velocity (WHSV) of 0.87 h^{-1}. The effluents (benzene, toluene, ethylbenzene, and styrene) were collected by test tube in an ice water bath and then analyzed by using gas chromatography (East & West Analytical Instruments GC-4000A) equipped with an FID detector. The EB conversion and ST selectivity were calculated based on the following respective equations:

$$\text{EB conversion}\,(\%) = \frac{EB_{inlet} - EB_{outlet}}{EB_{inlet}} \times 100\% \quad (1)$$

$$\text{ST selectivity}\,(\%) = \frac{ST_{outlet}}{Ben_{outlet} + Tol_{outlet} + ST_{outlet}} \times 100\% \quad (2)$$

where EB, ST, Tol, and Ben are the abbreviations for ethylbenzene, styrene, toluene, and benzene, respectively.

3 Results and discussion

3.1 Catalyst characterization

Figure 1 illustrates the XRD patterns of all the catalysts which were annealed at 550 ℃ for 6 h. It is distinctly observed that the crystalline structure and dispersion of the active phase In_2O_3 are profoundly affected by several different supports. As in the case of In_2O_3/MgO, except for the well-defined Bragg reflections of the periclase phase MgO (JCPDS: 87-0652), feeble diffraction lines at 2θ = 30.9° and 32.8° can be indexed to the corundum-type structure of In_2O_3 (rh-In_2O_3, rh = rhombohedral, JCPDS: 22-0336) [31]. However, the strong diffraction peaks at 2θ = 30.6°, 35.5°, 45.7°, 51.2°, and 60.8° pertained to the cubic bixbyite-type In_2O_3 crystal structure (bcc-In_2O_3, bcc = body-centered cubic, JCPDS: 71-2194) [31] are observed for the In_2O_3/SiO_2 catalyst, indicating that the existence of a larger amount of the aggregated In_2O_3 oxides on the SiO_2 surface. As a sharp contrast with the above two catalysts, for the In_2O_3/Al_2O_3, in addition to some tiny peaks (2θ = 38.1° and 67.2°) of γ-Al_2O_3 phase (JCPDS: 75-0788), hardly discernible diffraction patterns characteristic of the In_2O_3 phase can be detected, revealing a well dispersion of the active phase. From Table 1, the average crystallite sizes of In_2O_3 over

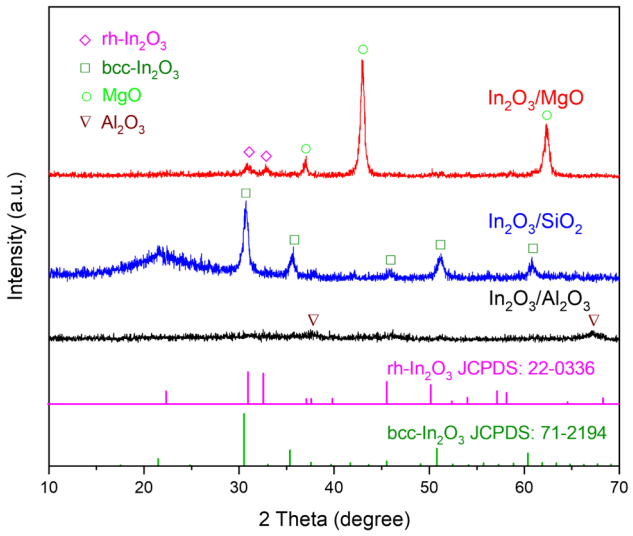

Fig. 1 XRD patterns of In_2O_3/MgO, In_2O_3/SiO_2, and In_2O_3/Al_2O_3 catalysts

MgO and SiO_2 supports calculated from the Scherrer Formula are 9.4 nm and 18.4 nm, respectively. Alternatively, because the characteristic diffraction peaks of In_2O_3 in the In_2O_3/Al_2O_3 catalyst have not been observed, so the corresponding crystalline size of In_2O_3 is not provided in Table 1. These results provide rich information that the support not only affects the dispersity of indium oxide but leads to the transformation of the crystalline phase.

Figure 2 provides the SEM and TEM images of the samples. As far as the catalyst support is concerned, MgO exhibits an octahedral-like morphology which is composed of large particles with a size of ~ 300 nm (Fig. 2A). These crystals as a support are rather dense and smooth. While the sponge-like morphology of SiO_2 and Al_2O_3 is comprised of a multitude of ultra-small nanoparticles that are further accumulated to form loosely porous structure (Fig. 2B and C). To identify the crystal structure of In_2O_3 on these supports, the representative micrographs based on the TEM experiments are portrayed in Fig. 2D–F. From Fig. 2D, the

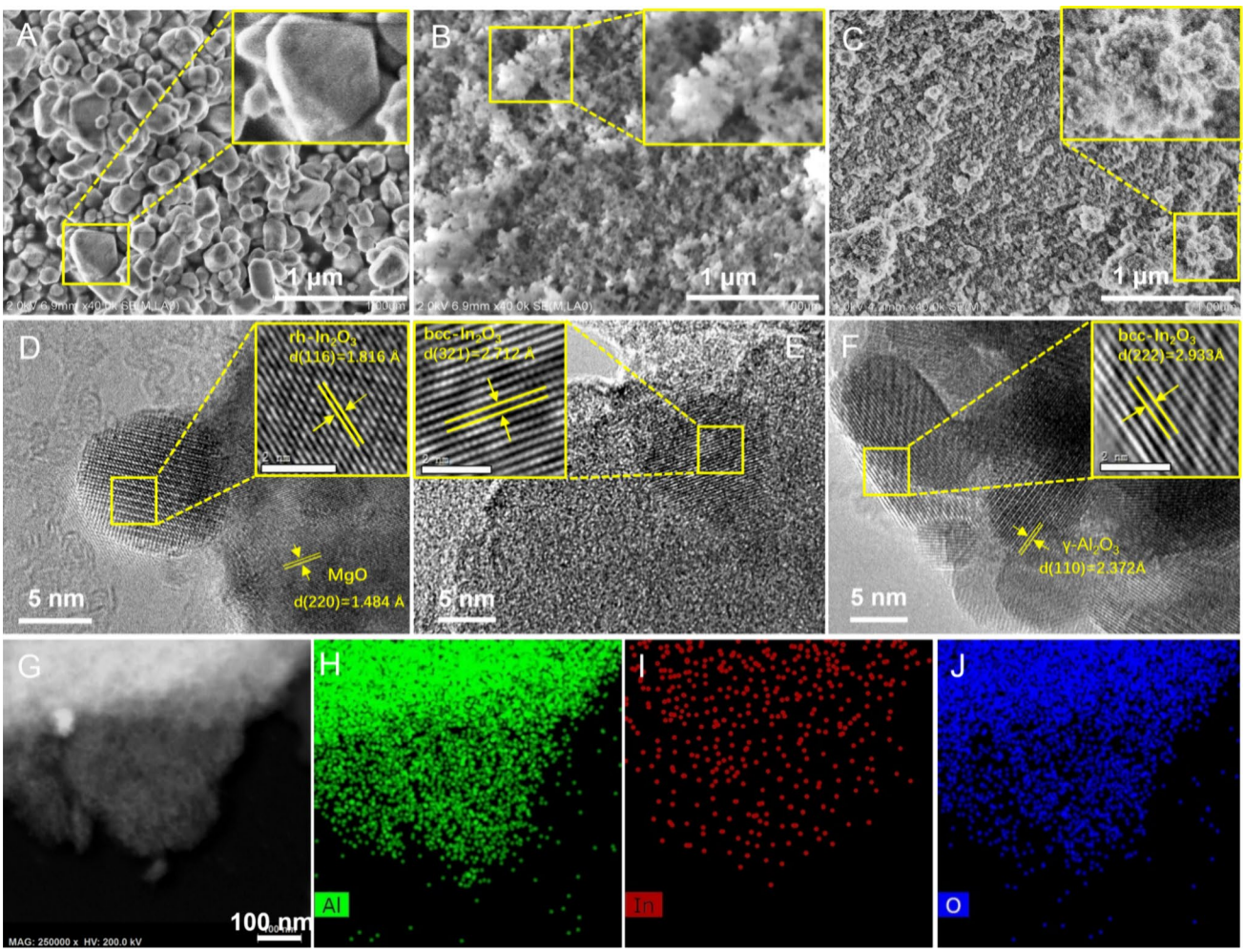

Fig. 2 **A**–**C** SEM and **D**–**J** TEM characterizations of samples: **A** MgO; **B** SiO_2; **C** Al_2O_3; **D** In_2O_3/MgO; **E** In_2O_3/SiO_2; **F** In_2O_3/Al_2O_3; **G** TEM image and **H**–**J** the corresponding elemental mapping images of In_2O_3/Al_2O_3

distance between the adjacent clear lattice stripes obtained by Fourier transform is 1.816 Å, which corresponds to the (116) plane of rh-In_2O_3 observed for the In_2O_3/MgO. However, as for both In_2O_3/SiO_2 and In_2O_3/Al_2O_3, the d spacings of lattice fringes are 2.712 Å and 2.933 Å, ascribing to the (321) and (222) planes of bcc-In_2O_3, respectively. Furthermore, the TEM-EDS mapping presents that the In element is homogeneously distributed on the In_2O_3/Al_2O_3 surface, and no apparently agglomerated In is formed (Fig. 2I), which agrees with the aforementioned XRD results.

The N_2 adsorption–desorption isotherm and corresponding pore size contribution (based on the NLDFT model) of the supports and supported In_2O_3 catalysts are shown in Fig. 3. The textural data are tabulated in Table 1. All samples display typical type-IV isotherm curves with narrow hysteresis loop, denoting a typical feature of mesoporous materials. In comparison with the bare support, the corresponding supported In_2O_3 catalyst shows similar isotherm and pore size distribution (Fig. 3) which implies that the loading of In_2O_3 does not impair the mesopore structure of the support. Nevertheless, among these In_2O_3/S catalysts, a notable distinction is the shape and starting position of the hysteresis loop. The hysteresis loop of In_2O_3/MgO and In_2O_3/SiO_2 can be grouped as type-H4 according to the IUPAC classification and the N_2 adsorption capacity at $P/P_0 > 0.85$ is steeply increased, alluding to the presence of split-shaped interstitial mesopores [32]. And the average pore diameters (D_{pore}) of In_2O_3/MgO and In_2O_3/SiO_2 are 24.1 nm and 25.2 nm, respectively. Different from the former ones, the In_2O_3/Al_2O_3 catalyst performs a type-H2 hysteresis loop, signifying a typical nearly tubular mesopore [32]. A narrow unimodal distribution is clearly seen, which approaches to the D_{pore} (Fig. 3D). It is further found that for the In_2O_3/Al_2O_3, the pore diameter mainly centered at 6.8 nm is visibly decreased in comparison with that of the pristine Al_2O_3, which denotes that the highly dispersed In species, as supported by the XRD results, are mostly located inside the pores on the internal wall rather than at the pore openings. To some extent, the regular mesopore channels anchored with metal sites contribute to the diffusion of

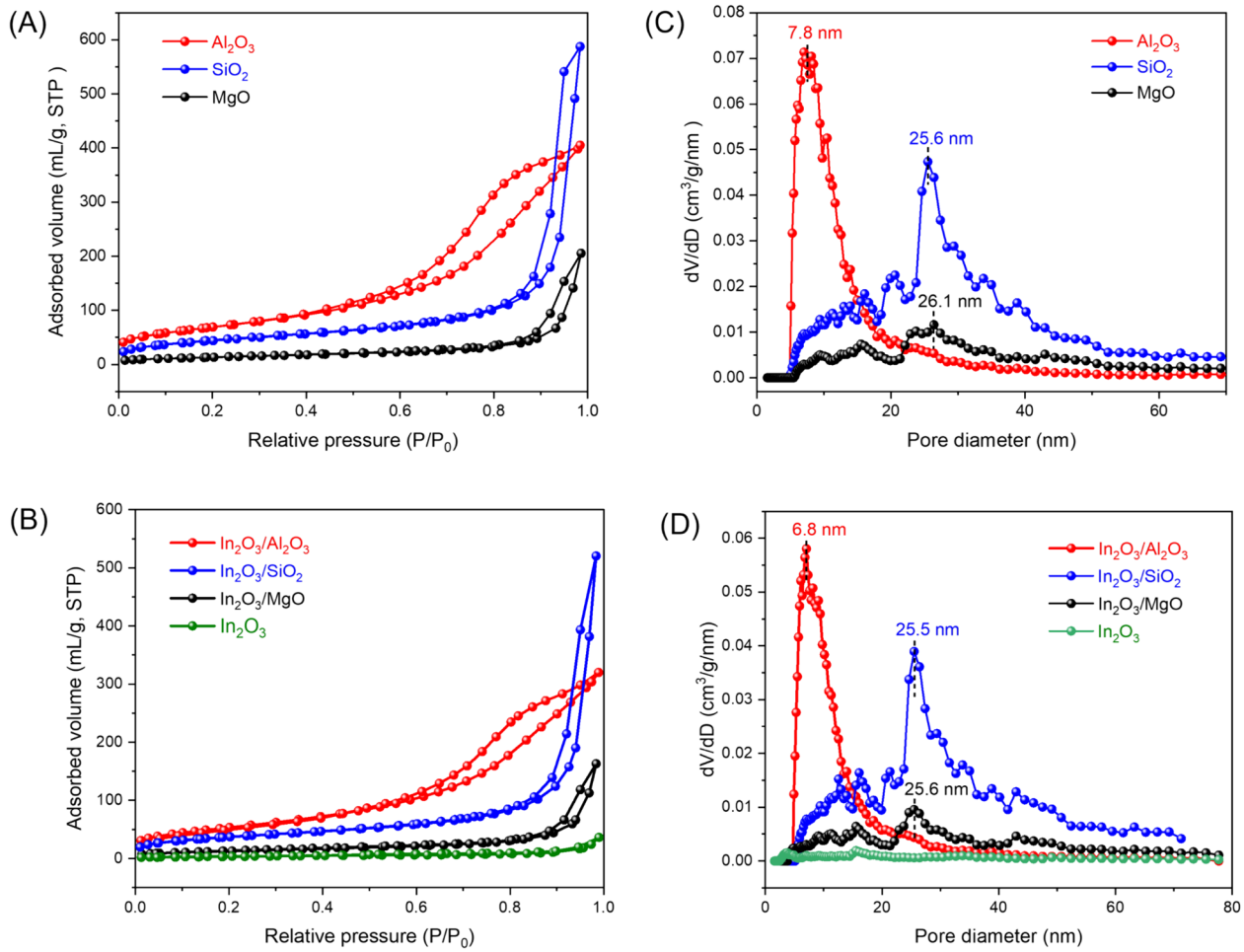

Fig. 3 **A**, **B** N_2 adsorption–desorption isotherm and **C**, **D** pore size distribution of samples

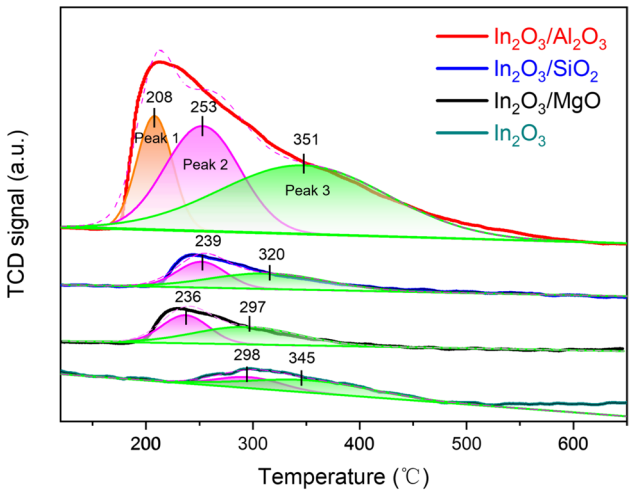

Fig. 4 NH_3-TPD spectra of In_2O_3/Al_2O_3, In_2O_3/SiO_2, In_2O_3/MgO, and In_2O_3

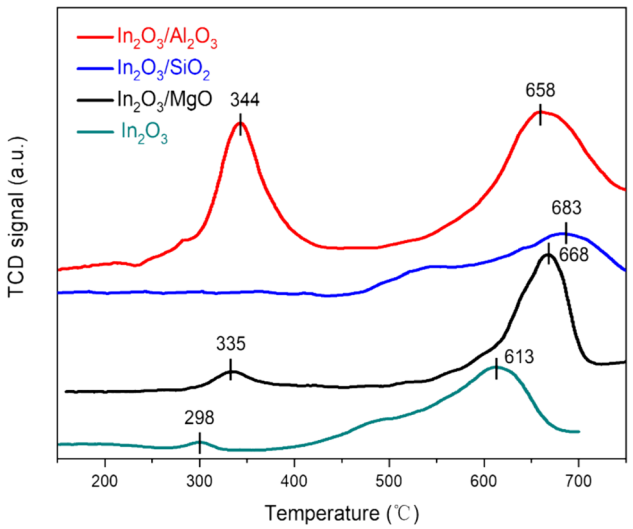

Fig. 5 CO_2-TPD profiles of In_2O_3/Al_2O_3, In_2O_3/SiO_2, In_2O_3/MgO, and In_2O_3

reactants and/or products when it comes to catalytic reaction [33]. Moreover, it can be seen from Table 1 that the BET surface area (S_{BET}) of Al_2O_3 support is significantly higher than that of both SiO_2 and MgO, which is more beneficial for better dispersion of In species.

The surface acid–base properties of the catalysts are of important features affecting the catalytic performance. Accordingly, NH_3- and CO_2-TPD experiments were carried out as displayed in Figs. 4 and 5, respectively. The number of acid and base sites can be well reflected by the desorption peak area. As shown in Fig. 4, only a feeble and broad NH_3 desorption peak of the bulk In_2O_3 can be found, representing that it has a little acidity. This also indicates that the acidity of the supported In_2O_3 catalyst depends notably on the type of support. As compared to In_2O_3/SiO_2 and In_2O_3/MgO with minor acidity, the In_2O_3/Al_2O_3 catalyst exhibits three extremely pronounced NH_3 desorption peaks (obtained by the Gaussian deconvolution method) centered at 208 ℃, 253 ℃ and 351 ℃, corresponding to weak, medium strength, and strong acid sites, respectively. Obviously, the Al_2O_3-supported In_2O_3 catalyst performs the highest overall acid sites amount among these catalysts. Figure 5 shows the surface basicity of the catalysts. The bulk In_2O_3 displays two CO_2 desorption peaks at 298 ℃ and 613 ℃, which indicates the existence of two types of basic sites, namely, medium strength basic sites and an abundance of strong basic sites, certifying the main basic feature of In_2O_3 [29]. The dominant desorption peak (> 660 ℃) attributed to strong basic sites is distinctly observed for all In_2O_3/S catalysts and the peak position shifts to a much higher temperature when compared to the bulk In_2O_3, revealing that the supported In_2O_3 catalysts have stronger basic sites. In comparison with In_2O_3/SiO_2 and In_2O_3/MgO, the In_2O_3/Al_2O_3 shows two CO_2 desorption peaks, which are centered at 344 ℃ and 658 ℃, respectively, which suggests that there are two different basic sites in the catalyst. In general, the amount of basic sites can be well reflected by the desorption peak area of CO_2. It can be seen from Fig. 5 that the total amount of basic sites for In_2O_3/Al_2O_3 catalyst is remarkably higher than that of In_2O_3/SiO_2 and In_2O_3/MgO. All the above results (Figs. 4 and 5) further indicate that the introduction of Al_2O_3 significantly modifies the acid–base distribution and increases both the overall acidity and basicity of the catalyst. The In_2O_3/Al_2O_3 catalyst has well-matched acidity and basicity which are conducive to the EB adsorption and CO_2 activation [30], respectively, effectively promoting the EB dehydrogenation reaction.

H_2-TPR measurements were executed to investigate the redox properties of the supported In_2O_3 catalysts. The reduction profile of the catalysts is shown in Fig. 6. The pure In_2O_3 only shows a H_2 consumption peak with an onset at 600 ℃ and maximum at 875 ℃, which is not entirely finished at the end of temperature. A similar profile is observed for the In_2O_3/MgO and In_2O_3/SiO_2 catalysts, but the maximum of the peak is shifted to a lower temperature (~ 740 ℃). It is worth noting that the In_2O_3/Al_2O_3 catalyst exhibits two well-marked reduction peaks, that is, the first peak is centered at 376 ℃ which is not seen in the other two catalysts and the second peak (590 ℃) is significantly shifted toward to a lower temperature than that of the abovementioned catalysts. According to the previous reports [34], these two typical reduction peaks are generally correlated to the sizes of In_2O_3 particles, with the highly dispersed In_2O_3 being reduced at low temperature and the bulk In_2O_3 being reduced at high temperature, respectively. As remarked above, compared to In_2O_3/MgO and In_2O_3/SiO_2 catalysts with the only existence of the bulk In_2O_3 particles, the larger amount of highly

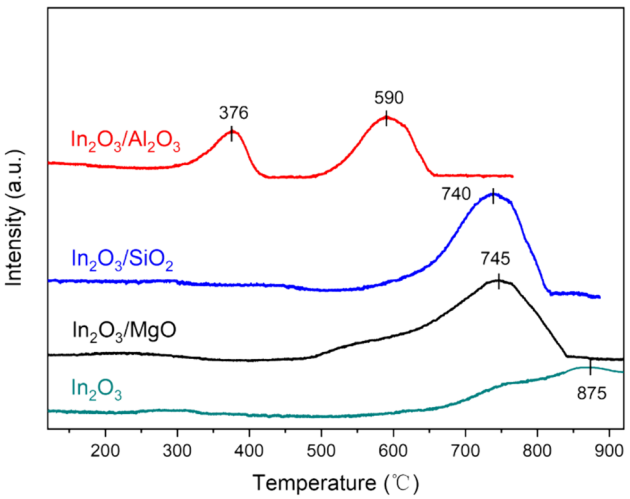

Fig. 6 H_2-TPR profiles of In_2O_3/Al_2O_3, In_2O_3/SiO_2, In_2O_3/MgO, and In_2O_3

dispersed In species except for the bulk one is formed when Al_2O_3 is selected as support.

3.2 Dehydrogenation activities

The catalytic performances of the different catalysts for EBDH-CO_2 are performed in Fig. 7. As for this reaction, the main product formed is styrene and the minor by-products are benzene and toluene. As seen from Fig. 7A, all catalysts exhibit high selectivity to ST (> 97%), indicating that there are only minor side reactions. Whereas, the EB conversion has a markedly difference, indicating an obvious support effect on the catalytic activity of the supported In_2O_3 catalyst. Unsupported In_2O_3 shows low EB conversion of < 10% with negligible reactivity. An analogous catalytic behavior is also observed over the In_2O_3/SiO_2, which may be due to that it has poor dispersal of the active species (Fig. 1). This also indicates that the bulk In_2O_3 may not be the main active site for EBDH-CO_2. In sharp contrast, the EB conversions over In_2O_3/MgO and In_2O_3/Al_2O_3 (especially the latter) are considerably improved. And the catalytic activity of the In_2O_3/S catalysts increases in the order of $In_2O_3 \approx In_2O_3/SiO_2 < In_2O_3/MgO < In_2O_3/Al_2O_3$. It is further observed from Fig. 7B that the total converted amount of EB over In_2O_3/Al_2O_3 is 48.00 mmol/g_{cata} after reaction for 12 h, which is greatly higher than that of In_2O_3/MgO, In_2O_3/SiO_2, and In_2O_3 (18.52, 3.93, and 3.83 mmol/g_{cata}, respectively), indicating that the former maintains the high catalytic efficiency during the whole rection. Further on, the In_2O_3/Al_2O_3 catalyst is selected for investigation owing to its superior catalytic activity. The stability test for In_2O_3/Al_2O_3 was thus executed in Fig. 8. The fair stability with EB conversion declines from 41.7% to 32.7% reaching up to 37 h, which implies that observing the deactivation of the catalyst is a slow process. Besides, some interesting findings presented in Figs. 7A and 8 are that compared with the EB conversion of In_2O_3/MgO and In_2O_3/SiO_2 that has a continuing downward trend during the course of reaction, the In_2O_3/Al_2O_3 gives the best catalytic activity after undergoing an induction period of ~ 6 h, achieving a maximum EB conversion of ~ 52% which then remains almost unaltered throughout the 6 h testing period. Based on the earlier reports involving the alkanes dehydrogenation (in the CO_2 atmosphere) of In_2O_3-based catalysts [21, 26], such unique induction period should be belonged to the metallic In^0 formed during the reaction as the intrinsic active center resulted from the reduction of the well-dispersed In_2O_3 on the Al_2O_3 support. To further confirm this hypothesis, the fresh In_2O_3/Al_2O_3 was pretreated by 10% H_2/Ar at 450 ℃ for 2 h, ensuring that the well-dispersed In_2O_3 was utterly

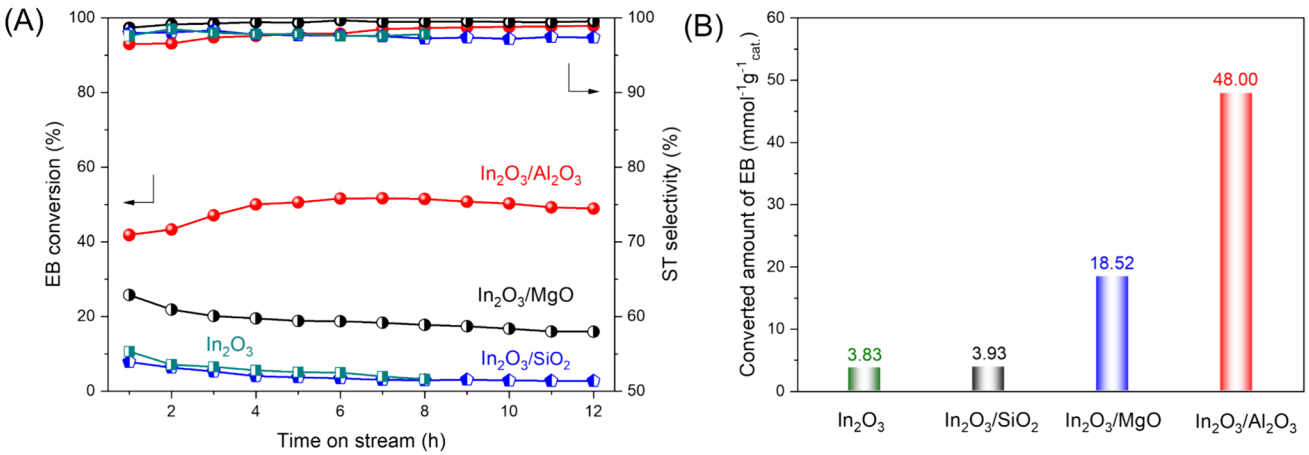

Fig. 7 **A** Conversion of EB and selectivity to ST and **B** converted EB amount over In_2O_3/Al_2O_3, In_2O_3/SiO_2, In_2O_3/MgO, and In_2O_3 catalysts in the presence of CO_2

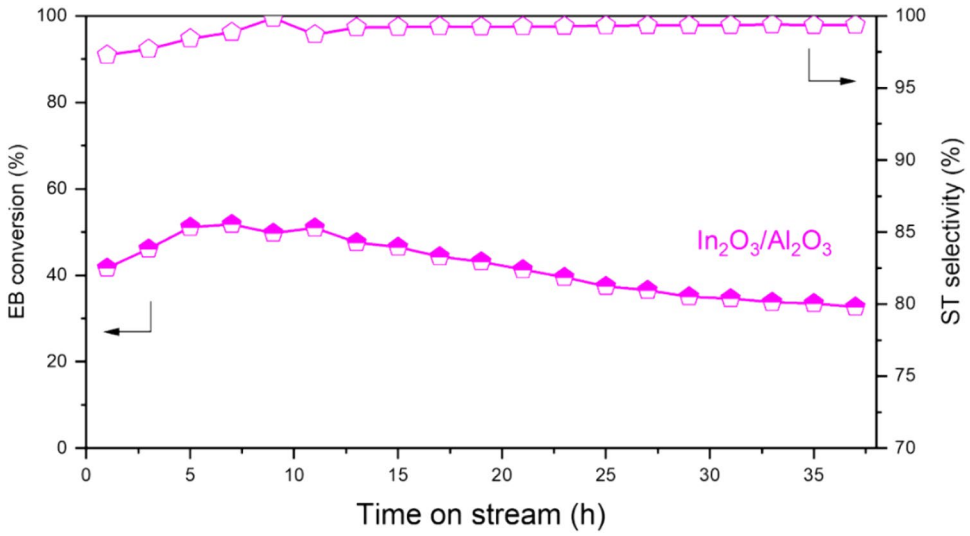

Fig. 8 The stability test for the dehydrogenation of EB under CO_2 over In_2O_3/Al_2O_3 catalyst

reduced according to the results of H_2-TPR as observed from Fig. 6. XPS was employed to investigate the valence states of In species before and after the catalyst treatment with H_2/Ar. $In3d_{5/2}$ photoelectron peak of the fresh In_2O_3/Al_2O_3 and reduced In_2O_3/Al_2O_3 (hereafter named In_2O_3/Al_2O_3-R) catalysts is depicted in Fig. 9. The peaks of $In3d_{5/2}$ at ~ 444.5 eV and ~ 443.5 eV can be respectively assigned to In^{3+} and In^0 species [21]. The XPS results confirm the existence of metallic In in the In_2O_3/Al_2O_3-R catalyst. Furthermore, by employing H_2 chemisorption experiment, it can be calculated that the dispersion of In_2O_3/Al_2O_3-R is 48.3%. The catalytic performance of the In_2O_3/Al_2O_3-R catalyst, shown in Fig. 10A, was tested under the identical reaction conditions. In line with the expectation, the induction period is nearly vanished and the initial EB conversion of In_2O_3/Al_2O_3-R is 56.2%, substantially higher than for In_2O_3/Al_2O_3 catalyst, thereby affirming that during the reaction process of EBDH-CO_2, the produced In^0 species by the reduction of highly dispersed In_2O_3 become the essential factor for enhancing the catalytic activity of EB.

To elucidate the effect of CO_2 on the EB dehydrogenation performance, the catalytic test was run over the In_2O_3/Al_2O_3 catalyst in the presence of N_2 (instead of CO_2) atmosphere. As portrayed in Fig. 10B. It is unexpected that although the selectivity of ST is well maintained at > 97%, the EB conversion of merely ~ 24% is obtained in the presence of N_2, which is more than half lower than that in the presence of CO_2 (Fig. 7A). It signifies that the promotion effect of CO_2 on this new In-catalyzed system is more obvious compared to the previously reported V-, Mo, and Fe-based catalysts [9, 35, 36].

As we all known, superior surface basicity is beneficial for the acidic molecules (such as CO_2) adsorption and consecutive reaction. In this study, the basic sites amount for In_2O_3/Al_2O_3 as revealed by CO_2-TPD (Fig. 5) is far superior relative to those for In_2O_3/MgO and In_2O_3/SiO_2 catalysts,

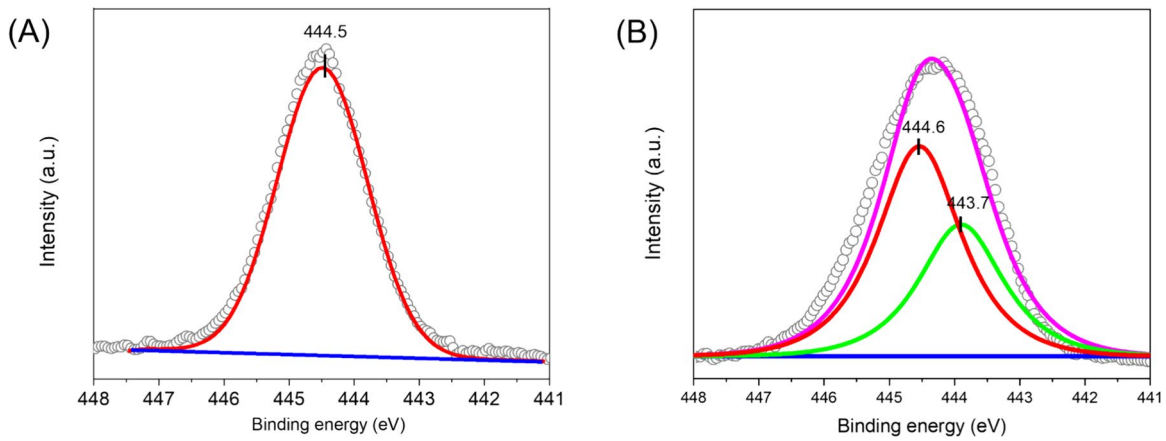

Fig. 9 $In3d_{5/2}$ XPS spectra of **A** the fresh In_2O_3/Al_2O_3 and **B** reduced In_2O_3/Al_2O_3 (In_2O_3/Al_2O_3-R)

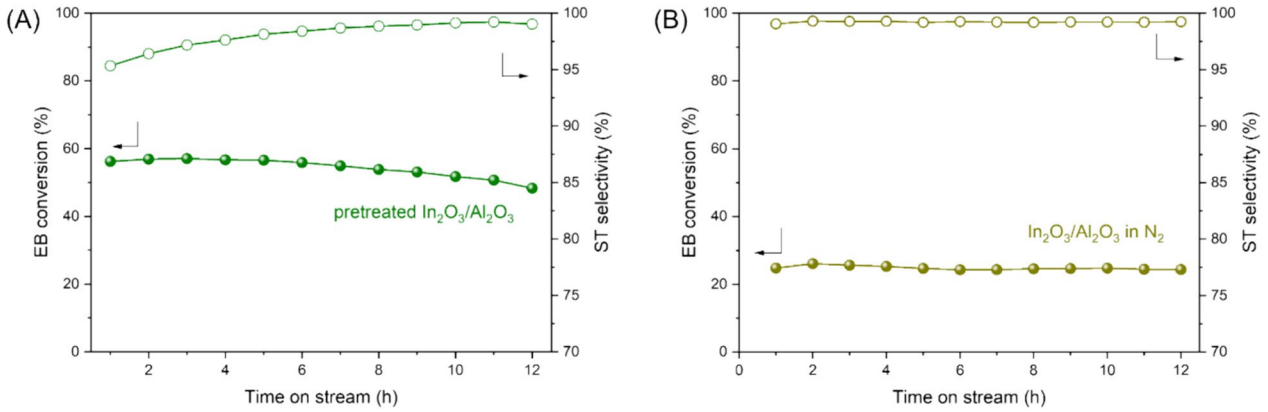

Fig. 10 **A** Conversion of EB and selectivity to ST over In_2O_3/Al_2O_3 pretreated by exposing H_2/Ar at 450 ℃ for 2 h. **B** Conversion of EB and selectivity to ST over In_2O_3/Al_2O_3 in the presence of N_2

which may well be responsible for RWGS reaction. As for this catalyst, bulk In_2O_3 other than Al_2O_3 is recognized as an active phase for RWGS reaction due to the former having higher basicity. Afterwards, this conclusion is well demonstrated by Chen et al. [21]. They found that during the process of RWGS reaction, for the 1073 K-reduced In-Al-20 catalyst, in which all In species were absolutely reduced at 1073 K in the presence of H_2/Ar atmosphere, dramatically lower CO yield was observed as compared to that of the fresh In-Al-20 and 773 K-reduced In-Al-20 catalysts (the only highly dispersed In_2O_3 was reduced at 773 K), which further certifies the bulk In_2O_3 performed as the active site for RWGS reaction.

It has been extensively acknowledged that the dehydrogenation of EB in the atmosphere of CO_2 can process through two different reaction pathways. The first one is a one-step pathway, that is, CO_2 promotes the dehydrogenation reaction, which can re-oxidize the catalyst surface as reduced by EB. This direct process is in line with the Mars-Van Krevelen redox cycle mechanism [37, 38]. That has been proposed for the Mo-, Cr-, V-, and Ce-based catalysts [35, 39–41]. The second one is a two-step process, which is a simple dehydrogenation, followed by the RWGS reaction. In this way, CO_2 can react with hydrogen from the reaction system, releasing the chemical equilibrium limitation and facilitating the styrene formation. Such the promotion role of CO_2 is often observed over the Fe-based catalysts [42–44]. To gain insight into the relationship of the structure–activity of the catalyst and further disclose the definite reaction pathway of this reaction, the redox properties of In_2O_3/Al_2O_3 are further investigated by H_2-TPR test. The designed proposal is that the well-dispersed In_2O_3 in the In_2O_3/Al_2O_3 catalyst was entirely reduced by rational controlling the reduction temperature of 450 ℃, based on the results of the first TPR (Fig. 6). After that, the weight of the reduced In_2O_3/Al_2O_3 (In_2O_3/Al_2O_3-R) catalyst is intentionally divided into two equal parts. The second TPR experiment of one part of the In_2O_3/Al_2O_3-R catalyst was executed under the same conditions as the first TPR. As observed from Fig. 11, the result shows that as for In_2O_3/Al_2O_3-R, the reduction peak in the high temperature (590 ℃) is still observed while that in the low temperature (376 ℃) completely disappears as compared to the fresh one, confirming that the well-dispersed In species have been thoroughly reduced and the bulk In_2O_3 is still retained. The other part of the reduced catalyst was pretreated with CO_2 at 550 ℃ for 2 h, and then the third TPR was also carried out under the identical conditions. As a result, the low-temperature reduction peak of the CO_2-treated In_2O_3/Al_2O_3-R has not been detected yet, adequately indicating

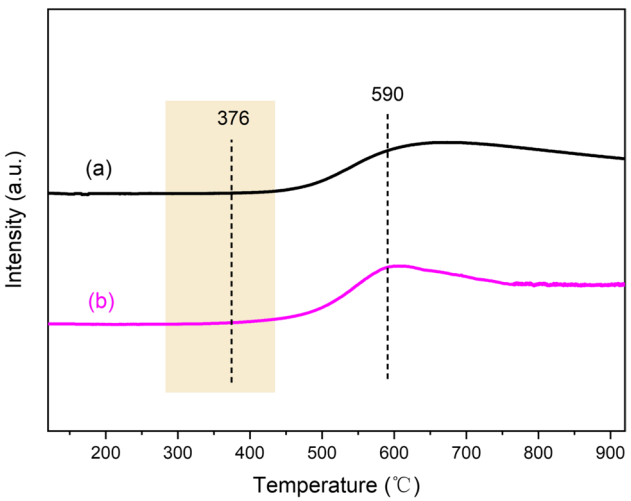

Fig. 11 H_2-TPR profiles of different catalysts: (a) In_2O_3/Al_2O_3 pretreated by 10 vol.% H_2/Ar at 450 ℃ for 2 h; (b) In_2O_3/Al_2O_3 pretreated by 10 vol.% H_2/Ar at 450 ℃ for 2 h followed by exposure to a flow of CO_2 (20 mL/min) at 550 ℃ for 2 h

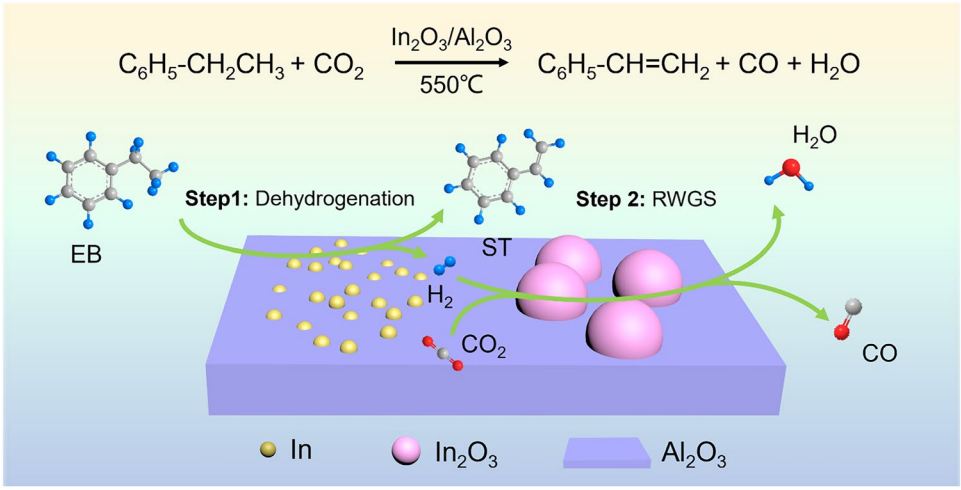

Scheme 1 Proposed reaction pathway of the EB dehydrogenation in CO_2 over In_2O_3/Al_2O_3 catalyst

that metallic In cannot be re-oxidized by CO_2. Combining with the above-mentioned catalytic data from Figs. 7A and 10, it is rational to speculate that the dehydrogenation of EB in the presence of CO_2 over In_2O_3/Al_2O_3 catalyst may proceed via the two-step pathway, namely, the direct dehydrogenation of EB occurs on the metallic In as the main active center and then the generated hydrogen can react with CO_2 through RWGS reaction, which takes place on the bulk phase In_2O_3. The synergistic effect of metallic In and the bulk In_2O_3 is well responsible for the satisfied catalytic performance. Scheme 1 intuitively illustrates the proposed reaction pathway of the dehydrogenation of EB in CO_2 over In_2O_3/Al_2O_3 catalyst.

To further provide insights into the chemical and structural changes of the active species during the ethylbenzene dehydrogenation with CO_2 reaction, the fresh and spent In_2O_3/S (S = Al_2O_3, MgO, and SiO_2) catalysts were further characterized using XPS measurement. As can be seen from Fig. S1, compared to the fresh In_2O_3/S catalysts, the $In3d_{5/2}$ spectra of all the spent catalysts are deconvoluted into two specifics: one at a higher binding energy of 444.4–444.6 eV attributing to the oxidation state of indium and the other at a lower binding energy of 443.7 eV corresponding to the formation of metallic In. From Table S1, in the case of In_2O_3/Al_2O_3 catalyst, the percentage of metallic In (28.6%) is obviously higher than that of In_2O_3/SiO_2 and In_2O_3/MgO (7.1% and 9.4%, respectively). This indicates that during the reaction, the partial In_2O_3 can be reduced to metallic In under the current reaction conditions and the amount of metallic In positively correlates with that of the highly dispersed In_2O_3 (Fig. 6). Moreover, combining with the above-mentioned proposed reaction mechanism (Scheme 1) and catalytic data from Fig. 7, these results further reveal that the optimal proportion of In and In_2O_3 may be better to balance the EBDH and RWGS reactions so as to achieve efficient conversion of EB.

4 Conclusions

The dehydrogenation of EB in the presence of CO_2 was systematically investigated over three In-based catalysts with different supports. As compared to SiO_2 and MgO, Al_2O_3 had been demonstrated to be the most effective support for dispersing In_2O_3 aggregates well, as it can be used to fabricate a highly active and stable dehydrogenation catalyst. The better dispersal of In_2O_3 on the Al_2O_3 surface was verified by XRD, TEM, and H_2-TPR studies. The catalytic tests for the EBDH-CO_2 showed that the In_2O_3/Al_2O_3 catalyst boosted the catalytic performances achieving the high EB conversion of 51.6% and ST selectivity of > 97%, which can be principally ascribed to the synergistic effect of metallic In and bulk In_2O_3. This work also provides a new pathway for designing a more efficient catalyst for DHEB-CO_2.

Supplementary Information The online version contains supplementary material available at https://doi.org/10.1007/s10934-024-01633-5.

Acknowledgements This work was supported by the National Natural Science Foundation of China (No. 22378286), Funds for Central Government to Guide Local Science, Technology Development (No. YDZJSX2021A014), Natural Science Foundation of Higher Education Institutions of Anhui Province (2022AH050967), Anhui Provincial Natural Science Foundation (2008085QB91), and Jiangsu Provincial Natural Science Foundation (BK20210001).

Author contributions Q. W.: Conceptualization; Project administration; Writing - original draft R. W.: Investigation; Methodology M. P.: Software; Data curation; Funding acquisition Y. L.: Formal analysis; Conceptualization L. Z.: Data curation J. Z.: Validation; Visualization S. C.: Supervision; Writing - review & editing; Project administration Y. Z.: Funding acquisition H. W.: Investigation K. Y.: Conceptualization Y. Y.: Methodology; Validation J. L.: Software

Declarations

Competing interests The authors declare no competing interests.

References

1. J. Diao, M. Hu, Z. Lian, Z. Li, H. Zhang, F. Huang, B. Li, X. Wang, D.S. Su, H. Liu, $Ti_3C_2T_x$ MXene catalyzed ethylbenzene dehydrogenation: active sites and mechanism exploration from both experimental and theoretical aspects. ACS Catal. **8**, 10051–10057 (2018)
2. F.D. Mango, The light hydrocarbons in petroleum: a critical review. Org. Geochem. **26**, 417–440 (1997)
3. L. Wang, Y. Wang, R. Zhang, R. Ding, X. Chen, B. Lv, Edge-activating CO_2-mediated ethylbenzene dehydrogenation by a hierarchical porous BN catalyst. ACS Catal. **10**, 6697–6706 (2020)
4. Y. Li, J. Su, F. Yu, X. Yan, D. Pan, R. Li, Y. Yang, Dehydrogenation of ethylbenzene with CO_2 over porous Co/Al_2O_3-ZrO_2 catalyst. Mater. Chem. Phys. **257**, 123773 (2021)
5. X. Dai, T. Cao, X. Lu, Y. Bai, W. Qi, Tailored Pd/C bifunctional catalysts for styrene production under an ethylbenzene oxidative dehydrogenation assisted direct dehydrogenation scheme. Appl. Catal. B Environ. **324**, 122205 (2023)
6. K. Zhang, G. Cui, M. Yuan, H. Huang, N. Li, J. Xu, G. Wang, C. Li, Sn-decorated CeO_2 with different morphologies for direct dehydrogenation of ethylbenzene. J. Rare. Earth. **42**, 102–109 (2022)
7. J. Sheng, W. Li, W. Lu, B. Yan, B. Qiu, X. Gao, R. Zhang, S. Zhou, A. Lu, Preparation of oxygen reactivity-tuned FeO_x/BN catalyst for selectively oxidative dehydrogenation of ethylbenzene to styrene. Appl. Catal. B Environ. **305**, 121070 (2022)
8. S. Chen, Z. Qin, X. Xu, J. Wang, Structure and properties of the alumina-supported vanadia catalysts for ethylbenzene dehydrogenation in the presence of carbon dioxide. Appl. Catal. A: Gen. **302**, 185–192 (2006)
9. S. Chen, Z. Qin, A. Sun, J. Wang, Effects of Li promoter on the catalytic performance of Fe-Li/AC for ethylbenzene dehydrogenation in the presence of CO_2, Chinese. J. Catal. **30**, 359–364 (2009)
10. K.N. Rao, B.M. Reddy, B. Abhishek, Y.H. Seo, N. Jiang, S.E. Park, Effect of ceria on the structure and catalytic activity of V_2O_5/TiO_2-ZrO_2 for oxidehydrogenation of ethylbenzene to styrene utilizing CO2 as soft oxidant. Appl. Catal. B Environ. **91**, 649–656 (2009)
11. P. Zhang, H. Lu, Y. Zhou, L. Zhang, Z. Wu, S. Yang, H. Shi, Q. Zhu, Y. Chen, S. Dai, Mesoporous $MnCeO_x$ solid solutions for low temperature and selective oxidation of hydrocarbons. Nat. Commun. **166**, 8446–8455 (2015)
12. K. Ren, J. Song, Y.H. Song, H. Wang, Z. Liu, Z. Liu, J. Jiang, Z. Liu, Catalytic behavior of manganese oxides for oxidative dehydrogenation of ethylbenzene with carbon dioxide. J. CO2 Util. **22**, 63–70 (2017)
13. X. Ye, Y. Yue, C. Miao, Z. Xie, W. Hua, Z. Gao, Effect of modifiers on the activity of a Cr_2O_3/Al_2O_3 catalyst in the dehydrogenation of ethylbenzene with CO_2. Green Chem. **7**, 524–528 (2005)
14. Z. Zhang, T. Zeng, C. Wei, L. Song, C. Miao, Ce-promoted Fe-K-Mg catalyst and its application in dehydrogenation of ethylbenzene. Mole. Catal. **540**, 113058 (2023)
15. X. Wang, M. Zhang, J. Liu, T. Luo, Y. Qian, Shape- and phase-controlled synthesis of In_2O_3 with various morphologies and their gas-sensing properties. Sensor Actuat B-Chem. **137**, 103–110 (2009)
16. J. Gao, L. Wang, K. Kan, S. Xu, L. Jing, S. Liu, P. Shen, L. Li, K. Shi, One-step synthesis of mesoporous Al_2O_3-In_2O_3 nanofibres with remarkable gas-sensing performance to NO_x at room temperature. J. Mater. Chem .A. **2**, 949–956 (2014)
17. T. Waitz, T. Wagner, T. Sauerwald, C.-D. Kohl, M. Tiemann, Ordered mesoporous In_2O_3: synthesis by structure replication and application as a methane gas sensor. Adv. Funct. Mater. **19**, 653–661 (2009)
18. Z. Li, P. Zhang, T. Shao, X. Li, In_2O_3 nanoporous nanosphere: a highly efficient photocatalyst for decomposition of perfluorooctanoic acid. Appl. Catal. B Environ. **125**, 350–357 (2012)
19. F.N. Tuzluca, Y.O. Yesilbag, M. Ertugrul, Synthesis of In_2O_3 nanostructures with different morphologies as potential supercapacitor electrode materials. Appl. Surf. Sci. **427**, 956–964 (2018)
20. C. Wang, Y. Han, M. Tian, L. Li, J. Lin, X. Wang, T. Zhang, Main-group catalysts with atomically dispersed In sites for highly efficient oxidative dehydrogenation. J. Am. Chem. Soc. **144**, 16855–16865 (2022)
21. M. Chen, J. Xu, Y. Cao, H. He, K. Fan, J. Zhuang, Dehydrogenation of propane over In_2O_3-Al_2O_3 mixed oxide in the presence of carbon dioxide. J. Catal. **272**, 101–108 (2010)
22. P.C. Zonetti, V.L. Bridi, G.G. Gonzalez, C.R. Moreira, O.C. Alves, R.R. de Avillez, L.G. Appel, Isobutene from ethanol: describing the synergy between In_2O_3 and m-ZrO_2. ChemCatChem **11**, 4011–4020 (2019)
23. S. Tan, S.J. Kim, J.S. Moore, Y. Liu, R.S. Dixit, J.G. Pendergast, D.S. Sholl, S. Nair, C.W. Jones, Propane dehydrogenation over In_2O_3-Ga_2O_3-Al_2O_3 mixed oxides. ChemCatChem **8**, 214–221 (2015)
24. L.-L. Long, W.-Z. Lang, X. Yan, K. Xia, Y.-J. Guo, Yttrium-modified alumina as support for trimetallic PtSnIn catalysts with improved catalytic performance in propane dehydrogenation. Fuel Process. Technol. **146**, 48–55 (2016)
25. S. Tan, L.B. Gil, N. Subramanian, D.S. Sholl, S. Nair, C.W. Jones, J.S. Moore, Y. Liu, R.S. Dixit, J.G. Pendergast, Catalytic propane dehydrogenation over In_2O_3–Ga_2O_3 mixed oxides. Appl. Catal. A **498**, 167–175 (2015)
26. M. Chen, J.-L. Wu, Y.-M. Liu, Y. Cao, L. Guo, H.-Y. He, K.-N. Fan, Study in support effect of In_2O_3/MO_x (M=Al, Si, Zr) catalysts for dehydrogenation of propane in the presence of CO_2. Appl. Catal. A **407**, 20–28 (2011)
27. H. Yan, K. He, I.A. Samek, D. Jing, M.G. Nanda, P.C. Stair, J.M. Notestein, Tandem In_2O_3-Pt/Al_2O_3 catalyst for coupling of propane dehydrogenation to selective H_2 combustion. Science **371**, 1257–1260 (2021)
28. L.J. Burcham, I.E. Wachs, The origin of the support effect in supported metal oxide catalysts: in situ infrared and kinetic studies during methanol oxidation. Catal. Today **49**, 467–484 (1999)
29. A. Gervasini, J.A. Perdigon-Melon, C. Guimon, A. Auroux, An in-depth study of supported In_2O_3 catalysts for the selective catalytic reduction of NO_x: the influence of the oxide support. J. Phys. Chem. B **110**, 240–249 (2006)
30. H. Li, Y. Yue, C. Miao, Z. Xie, W. Hua, Z. Gao, Dehydrogenation of ethylbenzene and propane over Ga_2O_3-ZrO_2 catalysts in the presence of CO_2. Catal. Commun. **8**, 1317–1322 (2007)
31. S.S. Farvid, P.V. Radovanovic, Phase transformation of colloidal In2O3 nanocrystals driven by the interface nucleation mechanism: a kinetic study. J. Am. Chem. Soc. **134**, 7015–7024 (2012)
32. A. Martínez, G. Prieto, J. Rollán, Nanofibrous γ-Al2O3 as support for Co-based Fischer-Tropsch catalysts: pondering the relevance of diffusional and dispersion effects on catalytic performance. J. Catal. **263**, 292–305 (2009)
33. H. Wang, W. Zhu, G. Yang, Y. Zhang, Y. Song, N. Jiang, Z. Liu, Z. Liu, Insights into the oxidative dehydrogenation of ethylbenzene with CO_2 catalyzed by the ordered mesoporous V_2O_5-$Ce_{0.5}Zr_{0.5}O_2$-Al_2O_3. Ind. Eng. Chem. Res. **58**, 21372–21381 (2019)
34. J.A. Perdigon-Melon, A. Gervasini, A. Auroux, Study of the influence of the In_2O_3 loading on gamma-alumina for the development of de-NO_x catalysts. J. Catal. **234**, 421–430 (2005)
35. I. Kainthla, G.V.R. Babu, J.T. Bhanushali, K.S.R. Rao, B.M. Nagaraja, Development of stable MoO_3/TiO_2-Al_2O_3 catalyst for oxidative dehydrogenation of ethylbenzene to styrene using CO_2 as soft oxidant. J. CO2 Util. **18**, 309–317 (2017)

36. M.A. Betiha, A.M. Rabie, A.M. Elfadly, F.Z. Yehia, Microwave assisted synthesis of a VO_x modified disordered mesoporous silica for ethylbenzene dehydrogenation in presence of CO_2. Microporous Mesoporous Mater. **222**, 44–54 (2016)
37. P. Sharma, R. Dwivedi, R. Dixit, M. Batra, R. Prasad, Mechanism evolution for the oxidative dehydrogenation of ethyl benzene to styrene over V_2O_5/TiO_2 catalyst: computational and kinetic approach. RSC Adv. **5**, 39635–39642 (2015)
38. H. Sun, J. Zhang, K. Li, H. Wang, X. Zhu, Efficient oxidative dehydrogenation of ethylbenzene over K/CeO_2 with exceptional styrene yield. Catalysts **13**, 781–788 (2023)
39. C. Zhu, S. Chen, D. Pan, X. Cui, Y. Qiao, R. Li, Ordered mesoporous alumina-supported vanadium oxides as an efficient catalyst for ethylbenzene dehydrogenation to styrene with CO_2. Catal. Commun. **115**, 12–16 (2018)
40. Y. Sakurai, T. Suzaki, K. Nakagawa, N.O. Ikenaga, H. Aota, T. Suzuki, Oxidation capability of carbon dioxide in the dehydrogenation of ethylbenzene over vanadium oxide-loaded MgO catalyst. Chem. Lett. **29**, 526–527 (2000)
41. L. Zhang, Z. Wu, N.C. Nelson, A.D. Sadow, I.I. Slowing, S.H. Overbury, Role of CO_2 as a softoxidant for dehydrogenation of ethylbenzene to styrene over a high-surface-area ceria catalyst. ACS Catal. **5**, 6426–6435 (2015)
42. S. Chen, A. Sun, Z. Qin, J. Wang, Reaction coupling of diethylbenzene dehydrogenation with water-gas shift over alumina-supported iron oxide catalysts. Catal. Commun. **4**, 441–447 (2003)
43. A. Sun, Z. Qin, J. Wang, Reaction coupling of ethylbenzene dehydrogenation with water-gas shift. Appl. Catal. A: Gen. **234**, 179–189 (2002)
44. S. Chen, Z. Qin, A. Sun, J. Wang, Theoretical and experimental study on reaction coupling:dehydrogenation of ethylbenzene in the presence of carbon dioxide. J. Nat. Gas Chem. **15**, 11–20 (2006)